**a**

| Virus | Clade | Tier | R1 IgG |
|---|---|---|---|
| Q23.17 | A | 1B | 67.76 |
| 94UG103 | A | 2 | 66.7 |
| 0260.v5.c36 | A | 2 | >500 |
| BaL.26 | B | 1B | 13.73 |
| 92BR020 | B | 2 | 66.7 |
| YU2.DG | B | 2 | 139.76 |
| 93IN905 | C | 2 | 22.2 |
| MGRM-C-026 | C | 2 | 22.2 |
| Du422.1 | C | 2 | 223.41 |
| ZM249M.PL1 | C | 2 | 194.4 |
| 3016.v5.c45 | D | 2 | >500 |
| X1193_c1 | G | 2 | >500 |
| X2131_C1_B5 | G | 2 | 201.22 |
| 6540.v4.c1 | AC | 2 | >500 |
| R2184.c04 | CRF01_AE | 2 | 81.27 |
| C2101.c01 | CRF01_AE | 2 | >500 |
| T250-4 | CRF02_AG | 2 | 261.22 |
| T257-31 | CRF02_AG | 2 | >500 |

**b**

| Virus | BaL.26 | Q23.17 |
|---|---|---|
| Clade | B | A |
| Tier | 1B | 1B |
| R1 IgG | 13.73 | 67.76 |
| gp140$^{YU2}$ depleted R1 IgG | >100 | >100 |

**c**

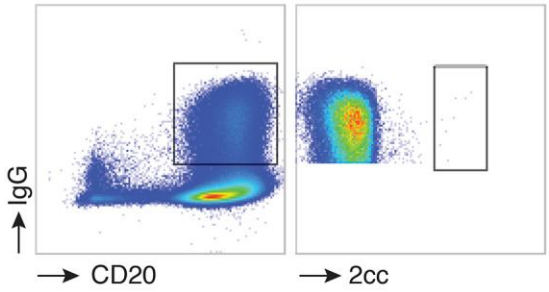


**d**

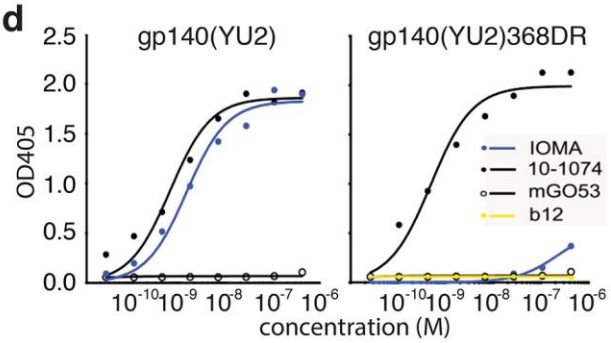


**e**

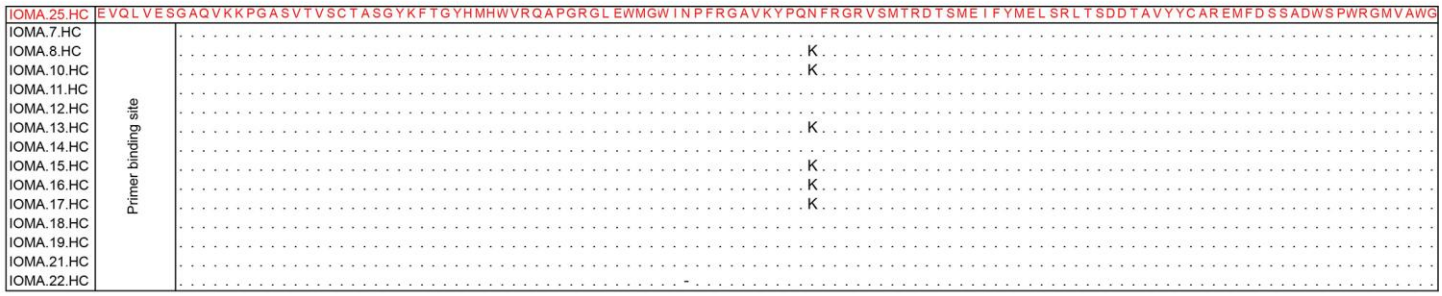



**Supplementary Figure 1**

Patient R1 serum analysis and isolation and characterization of IOMA.

(**a**) Neutralizing activity of purified serum IgG from patient R1 against a panel of 18 cross-clade HIV-1 viruses. Median inhibitory concentration ($IC_{50}$) of serum IgG indicated in red (1-50 μg/mL); orange (51-100 μg/mL); yellow (101-300 μg/mL); or white (>500 μg/mL). (**b**) Neutralizing activity of total R1 serum IgG versus $gp140^{YU2}$-absorbed R1 serum IgG against two HIV-1 viruses. (**c**) Representative flow cytometry plots for single cell-sorted 2cc-specific IgG+ B cells, pre-gated on total lymphocytes and singlets. (**d**) ELISAs measuring the binding of IOMA to wild-type $gp140^{YU2}$ (left) and to the CD4bs knockout $gp140^{YU2\ D368R}$ (right). Black lines with solid dots represent positive control antibody 10-1074; black lines with empty dot represent negative control antibody mGO53; blue lines represent IOMA; the yellow line represents the CD4bs antibody b12. (**e**) Clonal members of IOMA. Mature IOMA sequences are indicated in red. A dot indicates amino acid identity; a dash indicates an unclear residue in a sequence. Heavy chain clonal members (top). Light chain clonal members (bottom).

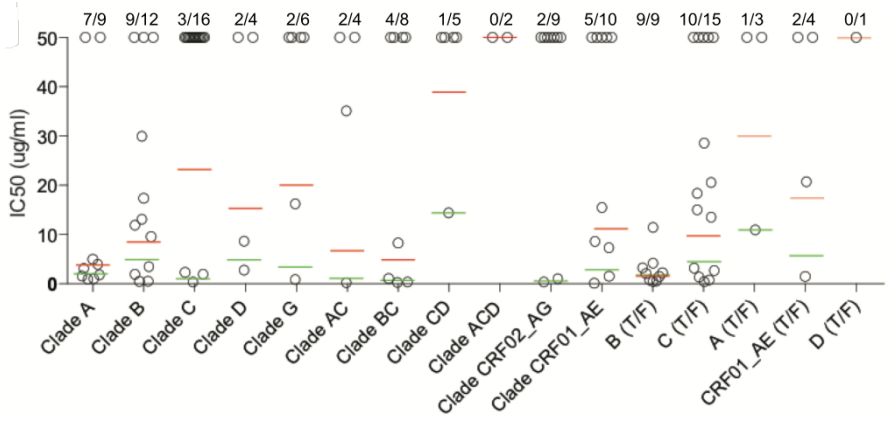


| | | Titer in TZM.bl cells (µg/ml) IOMA | |
|---|---|---|---|
| **Virus ID** | **Clade*** | **$IC_{50}$** | **$IC_{80}$** |
| 6535.3 | B | >50 | >50 |
| QH0692.42 | B | 12.890 | >50 |
| SC422661.8 | B | 17.346 | >50 |
| PVO.4 | B | 0.490 | 1.776 |
| TRO.11 | B | 0.539 | 1.948 |
| AC10.0.29 | B | >50 | >50 |
| RHPA4259.7 | B | 9.564 | >50 |
| THRO4156.18 | B | 29.741 | >50 |
| REJO4541.67 | B | >50 | >50 |
| TRJO4551.58 | B | 11.703 | >50 |
| WITO4160.33 | B | 3.259 | 26.793 |
| CAAN5342.A2 | B | 1.709 | 6.215 |
| | | | |
| WEAU_d15_410_787 | B (T/F) | 3.019 | 39.304 |
| 1006_11_C3_1601 | B (T/F) | 0.289 | 1.553 |
| 1054_07_TC4_1499 | B (T/F) | 2.209 | 7.665 |
| 1056_10_TA11_1826 | B (T/F) | 2.065 | 9.870 |
| 1012_11_TC21_3257 | B (T/F) | 0.347 | 1.253 |
| 6240_08_TA5_4622 | B (T/F) | 3.978 | 16.733 |
| 6244_13_B5_4576 | B (T/F) | 0.564 | 2.686 |
| 62357_14_D3_4589 | B (T/F) | 11.223 | >50 |
| SC05_8C11_2344 | B (T/F) | 1.465 | 5.589 |
| | | | |
| Du156.12 | C | >50 | >50 |
| Du172.17 | C | >50 | >50 |
| Du422.1 | C | >50 | >50 |
| ZM197M.PB7 | C | >50 | >50 |
| ZM214M.PL15 | C | 1.735 | 10.509 |
| ZM233M.PB6 | C | >50 | >50 |
| ZM249M.PL1 | C | >50 | >50 |
| ZM53M.PB12 | C | 2.316 | 15.303 |
| ZM109F.PB4 | C | >50 | >50 |
| ZM135M.PL10a | C | >50 | >50 |
| CAP45.2.00.G3 | C | >50 | >50 |
| CAP210.2.00.E8 | C | >50 | >50 |
| HIV-001428-2.42 | C | >50 | >50 |
| HIV-0013095-2.11 | C | 0.144 | 1.699 |
| HIV-16055-2.3 | C | >50 | >50 |
| HIV-16845-2.22 | C | >50 | >50 |
| | | | |
| Ce1086_B2 | C (T/F) | 0.556 | 8.351 |
| Ce0393_C3 | C (T/F) | 14.803 | >50 |
| Ce1176_A3 | C (T/F) | 2.961 | 12.584 |
| Ce2010_F5 | C (T/F) | 20.362 | >50 |
| Ce0682_E4 | C (T/F) | 1.155 | 16.081 |
| Ce1172_H1 | C (T/F) | >50 | >50 |
| Ce2060_G9 | C (T/F) | >50 | >50 |
| Ce703010054_2A2 | C (T/F) | >50 | >50 |
| BF1266.431a | C (T/F) | 28.336 | >50 |
| 246F C1G | C (T/F) | >50 | >50 |
| 249M B10 | C (T/F) | 18.130 | >50 |
| ZM247v1(Rev-) | C (T/F) | >50 | >50 |
| 7030102001E5(Rev-) | C (T/F) | 13.298 | 46.729 |
| 1394C9G1(Rev-) | C (T/F) | 0.211 | 1.264 |
| Ce704809221_1B3 | C (T/F) | 2.490 | 21.352 |
| | | | |
| CNE19 | BC | >50 | >50 |
| CNE20 | BC | 0.044 | 0.368 |
| CNE21 | BC | 1.062 | 20.087 |
| CNE17 | BC | >50 | >50 |
| CNE30 | BC | 8.291 | 46.591 |
| CNE52 | BC | >50 | >50 |
| CNE53 | BC | 0.127 | 0.769 |
| CNE58 | BC | >50 | >50 |

| | | Titer in TZM.bl cells (µg/ml) IOMA | |
|---|---|---|---|
| **Virus ID** | **Clade*** | **$IC_{50}$** | **$IC_{80}$** |
| MS208.A1 | A | 3.732 | 44.580 |
| Q23.17 | A | 0.833 | 3.309 |
| Q461.e2 | A | >50 | >50 |
| Q769.d22 | A | 1.363 | 8.114 |
| Q259.d2.17 | A | >50 | >50 |
| Q842.d12 | A | 2.882 | 19.480 |
| 3415.v1.c1 | A | 0.710 | 4.166 |
| 3365.v2.c2 | A | 4.986 | >50 |
| 0260.v5.c36 | A | 1.587 | 5.887 |
| | | | |
| 191955_A11 | A (T/F) | >50 | >50 |
| 191084 B7-19 | A (T/F) | 10.737 | >50 |
| 9004SS_A3_4 | A (T/F) | >50 | >50 |
| | | | |
| T257-31 | CRF02_AG | >50 | >50 |
| 928-28 | CRF02_AG | >50 | >50 |
| 263-8 | CRF02_AG | 0.827 | 6.123 |
| T250-4 | CRF02_AG | >50 | >50 |
| T251-18 | CRF02_AG | >50 | >50 |
| T278-50 | CRF02_AG | >50 | >50 |
| T255-34 | CRF02_AG | >50 | >50 |
| 211-9 | CRF02_AG | >50 | >50 |
| 235-47 | CRF02_AG | 0.159 | 0.623 |
| | | | |
| 620345.c01 | CRF01_AE | >50 | >50 |
| CNE8 | CRF01_AE | >50 | >50 |
| C1080.c03 | CRF01_AE | 15.291 | >50 |
| R2184.c04 | CRF01_AE | >50 | >50 |
| R1166.c01 | CRF01_AE | 8.409 | 39.033 |
| C2101.c01 | CRF01_AE | 1.519 | 9.150 |
| C3347.c11 | CRF01_AE | 0.097 | 0.440 |
| C4118.c09 | CRF01_AE | 7.096 | >50 |
| CNE5 | CRF01_AE | >50 | >50 |
| BJOX009000.02.4 | CRF01_AE | >50 | >50 |
| | | | |
| BJOX015000.11.5 | CRF01_AE (T/F) | >50 | >50 |
| BJOX010000.06.2 | CRF01_AE (T/F) | >50 | >50 |
| BJOX025000.01.1 | CRF01_AE (T/F) | 1.468 | 28.723 |
| BJOX028000.10.3 | CRF01_AE (T/F) | 20.540 | 38.852 |
| | | | |
| X1193_c1 | G | >50 | >50 |
| P0402_c2_11 | G | 16.024 | >50 |
| X1254_c3 | G | >50 | >50 |
| X2088_c9 | G | | |
| X2131_C1_B5 | G | >50 | >50 |
| P1981_C5_3 | G | >50 | >50 |
| X1632_S2_B10 | G | 0.641 | 5.105 |
| | | | |
| 3016.v5.c45 | D | >50 | >50 |
| A07412M1.vrc12 | D | 8.447 | >50 |
| 231965.c01 | D | >50 | >50 |
| 231966.c02 | D | 2.566 | 43.623 |
| | | | |
| 191821_E6_1 | D (T/F) | >50 | >50 |
| | | | |
| 3817.v2.c59 | CD | 14.208 | >50 |
| 6480.v4.c25 | CD | >50 | >50 |
| 6952.v1.c20 | CD | >50 | >50 |
| 6811.v7.c18 | CD | >50 | >50 |
| 89-F1_2_25 | CD | >50 | >50 |
| | | | |
| 3301.v1.c24 | AC | 34.886 | >50 |
| 6041.v3.c23 | AC | <0.023 | 0.082 |
| 6540.v4.c1 | AC | >50 | >50 |
| 6545.v4.c1 | AC | >50 | >50 |
| | | | |
| 0815.v3.c3 | ACD | >50 | >50 |
| 3103.v3.c10 | ACD | >50 | >50 |

* (T/F): Transmitted / Founder Virus

**Supplementary Figure 2**

Neutralizing activity of IOMA.

Top, Clade-specific neutralizing activity of IOMA against a 118-virus panel. Geometric mean $IC_{50}$ value including non-neutralized strains is indicated for each set of viruses by a red line; the green line indicates the geometric mean $IC_{50}$ value calculated for only neutralized strains. The number of neutralized and total strains evaluated for each clade are indicated at the top of the panel. Bottom, Neutralizing activity of IOMA against a 118-virus panel. $IC_{50}$ and $IC_{80}$ values (μg/mL) are indicated for each virus. Fields in red indicate neutralization.

**a**

```
                 ──────────FR1──────────  ─────CDRH1─────  ──FR2──  ─────CDRH2─────  ──────────FR3──────────  ─────CDRH3─────  ──FR4──
HC                   5   10   15   20   25          30   35   40   45   50   55   60   65   70   75        80        85   90   95          100       105  110
VH1-2*02  QVQLVQSGAEVKKPGASVKVSCKASGY--------TF-TGYYMHWVRQAPGQGLEWMGWINPNSGGTNY-AQKFQGRVTMTRDTSI---STAYMELSRLRSDDTAVYYCAR----------------------
IOMA      E....E...Q.......T..T.............K.....H.........R..........FR.AVK..P.N.R...S.....M....EIF.......T...........EMFDS..SADWSPWRGMVAWGQGTLVTVSS
12A12     SQH.....TQ.......RI..Q.............S...D.VL..W.............K.VY.AR....RR....INFD..IYR....EI.F.D..G.......L.F...DGSGD......DTSWHLDPWGQGTLVTVSA
12A21     SQH.....TQ.......R...Q.................N.IL..W.............L.K.VF.AV....RQ....IQL...IYR....EI.FLD..G.............DESGD......DLKWHLHPWGQGTQVTVSP
3BNC117   ....L....A.T......R...E.............NI.RD.FI..W.........Q.V.....KT.QP.N.PRQ.....SL..HA.WDFDTFSF..D.KA.........F...QRS.........DYWDFDVWGSGTQVTVSS
NIH45-46  ..R.S...GQM....E.MRL..R.............E..LNCPIN.I.L....RRP.....LK.RG.AV....R...........VYS....D..FL..RS.T.......F.T.GKYCT..ARD.YYNWDFEHWGRGAPVTVSS
VRC-CH30  .........A.R......T....FAEDDDYSPHWVNPA.PEH.I.FL......Q...LA.M..TN.AV....WQLH..L.A...G.M....T..FL.VRS.............AQKRG......RSEWAYAHWGQGTPVAVSS
VRC-CH31  .........A.R......T....FAEDDDYSPYWVNPA.PEHFI.FL......Q...LA.M..TN.AV....WYLN....A...R.M....T..FL.VKS.............AQKRG......RSEWAYAHWGQGTPVVVSS
VRC-CH32  .........A.R......T....FAEDDDFSPHWVNPA.PEH.I.FL......Q...LA.MK.TN.AV....WQL.....V...R.Q....T..FL.VKN.............AQKRG......RSEWAYAHWGQGTPVVISA
VRC-CH33  .........A.R.....IS....FADADDYSPHWMNPA.PEH.I.FL......Q...LA.M..TN.AV....WYLN....A...R.M....T..FL.VRS.............AQKRA......RSEWAYAHWGQGTPVVVSS
VRC-CH34  .........A.R......T....FAEDDDWSPHWVNPA.PEH.I.FL......Q...LA.M..TN.AV....WQLN..L.A.....M....T..FL.VKS.............AQKRG......RSEWAYAHWGQGTPVVVSS
VRC-PG04  ........SG.......R...WT.ED.........I.ERTELI.............I..VKTVT.AV.FGSPD.RQ..SL...RDL....F..H.DIRG.TQG...T.F...QKFYT.....GGQGWYFDLWGRGTLIVVSS
VRC-PG19  E.R..................R...A.................DFDI..L.....R.......VR.LG..VS...RQ...........FY.....D..F.DFRN.KM....L.F...MG..A.......AREWDFQYWGQGTRVLVSS
VRC-PG20  ..H.M...T.M.......R.T.QT..............SD.FI..L..V...R.F.....M..QW.QV....RT..........VYR....EV..LD.RS.TFA.....F...RMRSQ......DREWDFQHWGQGTRIIVSS
VRC01     ........GQM....E.MRI..R.............E..IDCTLN.I.L....KRP.....LK.RG.AV....RPL.........VYS....D..FL..RS.TV......F.T.GKNCD.......YNWDFEHWGRGTPVIVSS
VRC18     ........NQ.R......RI..E.............K..IDHFI.....V...H.....L.....RG..V...SRS...KL.....NFE....E...LD..K.NPG.....F...GFAG.........YEWSFIWGQGTLVIVSS
VRC23     ...F..............R...E.............S...D.VLQ.I.....RP......K.ER.AVS...PQ....L.L...LYT....E....HFKN.......I.....GVRRD.......ASWWLQFWGQGTLVTVSS
VRC27     ..R.....PQ.R...S..RI..ET..............NA.IL..F.....RSF.....K.KF.AV....HS....I.L...IYR....E..FLD.TG..............DRLYD......GSSWRLDYWGQGTRVVVSS

VH1-46*01 ..........................................S.....................I...SG.S.S.................T......V.....S...E.....................................
1B2530    ..R.E....AMR......TL..Q.............N..VK.II.....K..L.F..V.M.D.YR.RPWS..H.....LSLS....M....EIL..T.TS.K.....T.F...AEAAS...DSHSRPIMFDHWGQGSRVTVSS
1NC9      ..R......QL.......T...E.............N..VN.IIN....T..RSF..V.M.D.RR.RPWS.........L.L...IDS....EKL..H..G..G..........QDSDFHDGHGHTLRGMFDSWGQGSPVTVSS
8ANC131   .G......GGL....T..TI..L..E.............NEFVI..I.......PL.L.L.KRS-.RLMT..YN..D.LRLR..R.T....G.VF....RG...P..........DGLGE...V.APDYRYGIDVWGQGSTVIVTA
8ANC134   .G......GG.....T..TI..L..E.............NEFVI..I.......PV.L.L.KRS-.RLMT.SY...D.LSLR..R.T....G.VF....RG...L..........DGLGE...V.APAYLYGIDAWGQGSTVIVTS
CH235     ..................T...Q.................N..V.............QL....D.SW.R......N....I.......T......V....MRS...E.........NVATE......GSLLHYDYWGQGTLVTVSA
CH235.9   ..R.L.Y.GG..R....MTI..V.............N..ND..I.............L....D.SG.R.D...GA.GD..S.Y..K.M....N.L..D.RS...G...M...V.NVGTA......GSLLHYDHWGLGVMVTVSS
CH235.12  ....A.Y.GG..RL..TMTL..V.............ND..I..........F.LL.Y.D.AN.RPD...GALRE.LSFY..K.M....E.L..D.RS..Y....M...V.NVGTA......GSLLHYDHWGSGSPVIVSS
```

**b**

```
                 ──────────FR1──────────  ─CDRL1─  ─────FR2─────  ─────CDRL2─────  ──────────FR3──────────  ──CDRL3──  ─────FR4─────
LC                   5   10   15   20   25   30        35   40   45   50   55   60   65   70   75   80   85   90   95  100  105  110
LV2-23*02 QSALTQ-PASVSGSPGQSITISCTGTSSDVGSYNLVSWYQQHPGKAPKLMIYEVSKRPSGVSNRFSGSKSGNTASLTISGLQAEDEADYYCCSYAGS---STF-----------
KV1-33*01 DIQMTQSPSSLSASVGDRVTITCQASQD---IS-NYLNWYQQKPGKAPKLLIYDASNLETGVPSRFSGSGSGTDFTFTISSLQPEDIATYYCQQYD-----NL-----------
KV3-11*01 EIVLTQSPATLSLSPGERATLSCRASQS---VS-SYLAWYQQKPGQAPRLLIYDASNRATGIPARFSGSGSGTDFTLTISSLEPEDFAVYYCQQRS---NW-----------
KV3-20*01 EIVLTQSPGTLSLSPGERATLSCRASQS---VSSSYLAWYQQKPGQAPRLLIYGASSRATGIPDRFSGSGSGTDFTLTISRLEPEDFAVYYCQQYG---SS-----------

IOMA      QSALTQ-PASVSGSPGQSITISCAGSSRDVGGFDLVSWYQQHPGKAPKLIIYEVNKRPSGISSRFSASKSGNTASLTISGLQEEDEAHYYCYSYADG---VAFGGGTKLT-VLGQPKA
12A12     DIQMTQSPSSLSASVGDRVTITCQAGQG---IG-SSLQWYQQKPGKAPKLLVHGASNLHRGVPSRFSGSGFHTTFSLTISGLQRDDFATYFCAVLE-----FFGPGTKV--EIKRTVA
12A21     DIQMTQSPSSLSASVGDRVTINCQAGQG---IG-SSLNWYQKKPGRAPKLLVHGASNLQRGVPSRFSGSGFHTTFTLTISSLQPDDVATYFCAVFQ-----WFGPGTKV--DIKRT--
3BNC117   DIQMTQSPSSLSASVGDTVTITCQAN-G-----YLNWYQQRRGKAPKLLIYDGSKLERGVPSRFSGRRWGQEYNLTINNLQPEDIATYFCQVYE-----FVVPGTRL--DLKRTVA
NIH45-46  EIVLTQSPATLSLSPGETAIISCRTSQS-----GSLAWYQQRPGQAPRLVIYSGSTRAAGIPDRFSGSRWGADYNLSISNLESGDFGVYYCQQYE-----FFGQGTKVQVDIKRTVA
VRC-CH30  DIQMTQSPSSLSASLGDRVTITCQASRG---IG-KDLNWYQQKPGKAPKLLVSDASILEGGVPSRFSGSGFHQNFSLTISSLQPEDVATYFCQQYE-----TFGQGTKV--DIK----
VRC-CH31  DIQMTQSPSSLSASLGDRVTITCQASRG---IG-KDLNWYQQKAGKAPKLLVSDASTLEGGVPSRFSGSGFHQNFSLTISSLQAEDVATYFCQQYE-----TFGQGTKV--DIK----
VRC-CH32  DIQMTQSPSSLSASLGDRVTITCQASRG---IG-KDLNWYQQKPGRAPRLLVSDASILEGGVPTRFSGSGFHQNFSLTISSLQAEDVATYFCQQYE-----TFGQGTKV--DIK----
VRC-CH33  DIQMTQSPSSLSASLGDRVTITCQASRG---IG-KDLNWYQQKRGRAPRLLVSDASVLEGGVPSRFSGSGFHQNFSLTISTLQPEDVATYFCQQYE-----TFGQGTKV--DIK----
VRC-CH34  DIQMTQSPSSLSASLGDRVTITCQASRG---IG-KDLNWYQQKAGKAPKLLVSDASILEGGVPSRFSGSGFHQNFSLTISSLQPEDVATYFCQQYE-----TFGQGTKV--DIK----
VRC-PG04  EIVLTQSPGTLSLSPGETASLSCTAASY-----GHMTWYQKKPGQPPKLLIFATSKRASGIPDRFSGSQFGKQYTLTITRMEPEDFARYYCQQLE-----FFGQGTRL--EIRR---
VRC-PG19  QSALTQ-PASVSGSPGQSITISCTAS-SDFRGFSSVSWYQQVPGRAPKLLIFSVNRRPSGISHRFSGSKSGNTASLTISGLQIEDEADYHCNAYE-----FFGGTKVF-VLGQ---
VRC-PG20  QSALTQ-PPSVSGSPGQSITLSCTGAST-----SVAWYQQYADKAPRLIVFDGNKRPSDISSRFSGSQSGGTASLTISGLQSEDEAYYHCNAFE-----FFGGGTKLT-VLSQ---
VRC01     EIVLTQSPGTLSLSPGETAIISCRTSQY-----GSLAWYQQRPGQAPRLVIYSGSTRAAGIPDRFSGSRWGPDYNLTISNLESGDFGVYYCQQYE-----FFGQGTKVQVDIKR---
VRC18     EIVLTQSPGTLSLSPGETATLSCRTSQG---ILSNQLAWHQQRPGQPPRLLIYGGSNRAPGIPERFTGSGSGTDFVLTIKRLERDDFAVYYCQILE-----FFGRGTRV--EMN----
VRC23     EIVMTQSPVTVSVSRGGTATLSCRASQG---VG-SDVAWYQHKPGQTPRLLIYGASTRASGVPERFSGSGFHVDFTLSISGLQPEDVAIYYCQQYE-----TFGQGTKV--EIKRTVA
VRC27     DIQMTQSPSSLAVSVGGRVTITCRASQG---IG-SDLHWYQQKRGRPPILLIHDASAREEGVPSRFGGSGSHTPFIFTINDLQLDDVATYYCQVIE-----SFGQGTRL--DIN----

1B2530    QSALTQ-PPSASGAPGQRVTISCSGGPSNVGG-NYVYWYRQFPGTAPTLLILRDDQRPSGVPDRFSASKSGNSASLAISGLRPDDEGFYFCATYDSDGSIRLFGGGTALT-VLSQPKA
1NC9      NFMLTQ-VLSVSGTPGQRVIISCSGTSSNVGG-NLVSWYQHLPGAAPRLLIHRDDQRPSGVPDRFSGSKSGNSASLVISGLRSDDEADYFCAAYDSTFSLPVFGGGTRLT-VLSQPKA
8ANC131   EIVLTQSPATLSLSPGERATLSCRASQG---L--NFVVWYQQKRGQAPRLLIHAPSGRAPGVPDRFSARGSGTEFSLVISSVEPDDFAIYYCQEYSS--TPYNFGPGTRV--DRKRTVA
8ANC134   EIVLTQSPATLSLSPGERATLSCRASQG---L--NFVVWYQQKGGQAPRLLIHGPTDRAPGVPDRFSARGSGTEFSLVISSVEPDDFALYYCQEYSS--TPYNFGPGTRV--DRKRTVA
CH235     EIVLTQSPATLSVSPGERATLSCRASQS---VR-SNLAWYQQRPGQAPRLLIYGTSTRATGVPARFSGRGSGTEFTLAISSMQSEDFAVYLCLQYN---NWWTFGQGTKV--EIK----
CH235.12  EIVLTQSPATLSASPGERVTLTCRASRS---VR-NNVAWYQHKGGQSPRLLIYDASTRAAGVPARFSGSASGTEFTLAISNLESEDFTVYFCLQYN---NWWTFGQGTRV--DIK----
```

**c**

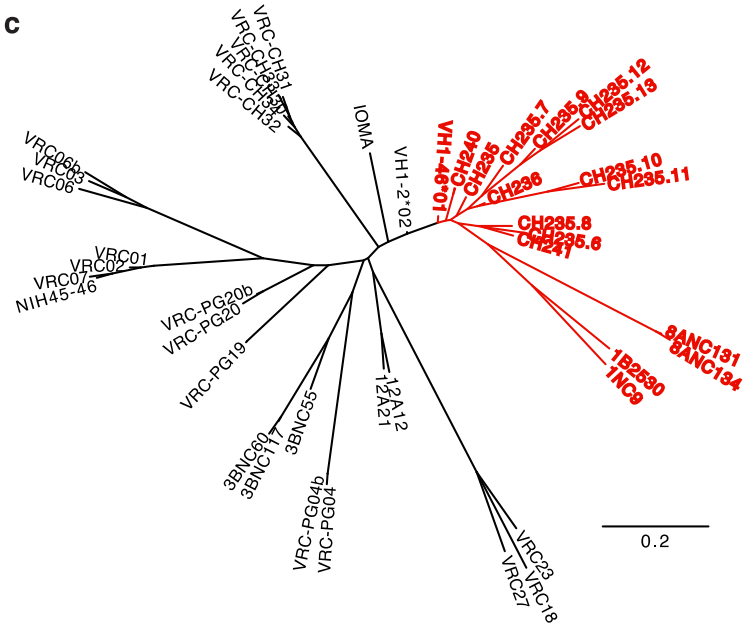

**Supplementary Figure 3**

Sequence alignment of CD4-mimetic bNAbs.

(**a**) Heavy chains. (**b**) Light chains. (**c**) Dendrogram showing relation of VH1-2 (black) and VH1-46 (red) CD4bs bNAbs. The dendrogram was calculated based on nucleotide sequence similarity of their aligned HC V gene segments. Scale bar represents 20% nucleotide substitutions per site.

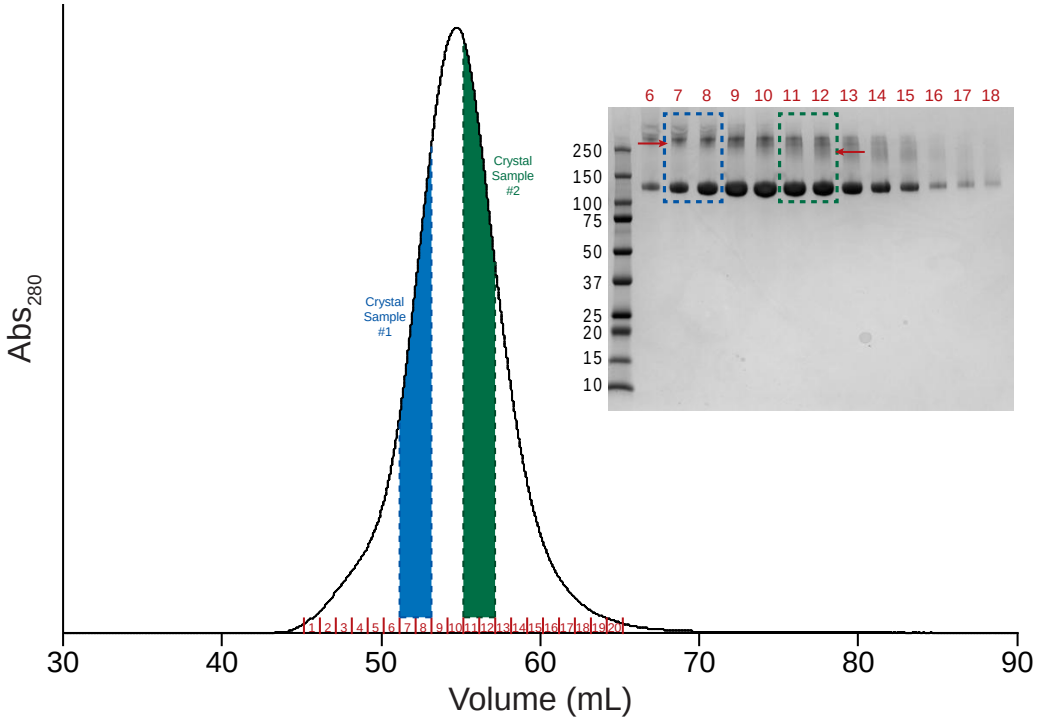
Abs280
Volume (mL)
30
40
50
60
70
80
90
Crystal Sample #1
Crystal Sample #2
6 7 8 9 10 11 12 13 14 15 16 17 18
250
150
100
75
50
37
25
20
15
10

**Supplementary Figure 4**

Characterization of BG505 SOSIP.664 protein used for crystallization.

Size exclusion chromatography (SEC) profile showing migration of the BG505 SOSIP.664 used for incubation with IOMA and 10-1074 Fabs to generate samples for crystallization. Inset shows SDS-PAGE analysis under non-reducing conditions of SEC fractions. SEC fractions 7-8 (blue) (larger apparent molecular mass; likely more glycosylated) were used for the 3.9Å IOMA–10-1074–BG505 structure and fractions 11-12 (smaller apparent molecular mass; likely less glycosylated) were used for the 3.5Å IOMA–10-1074–BG505 structure (Table 1).

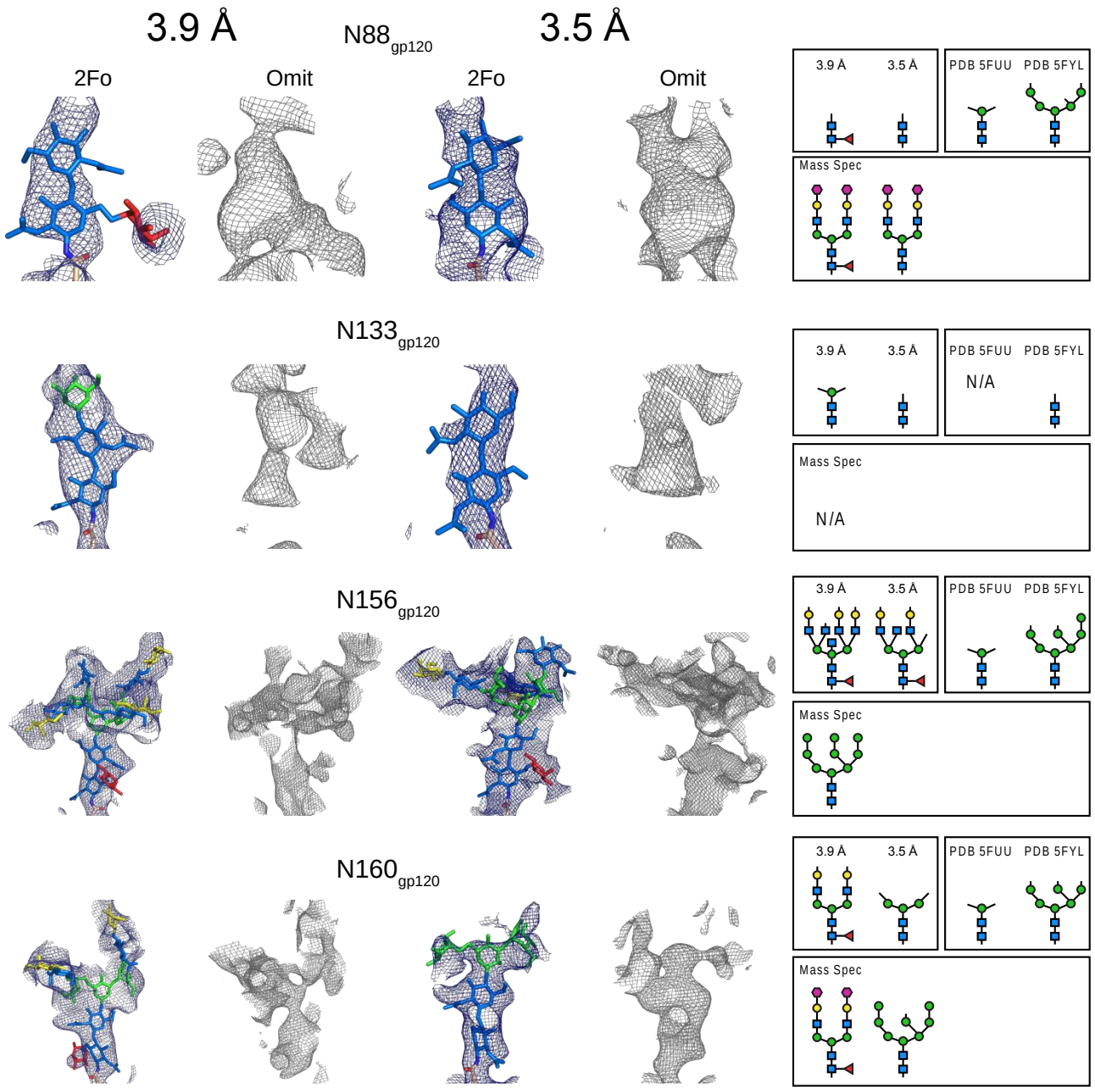


Nature Structural & Molecular Biology: doi:10.1038/nsmb.3291

**Supplementary Figure 5**

Glycans at individual BG505 SOSIP.664 PNGSs ($N88_{gp120}$–$N160_{gp120}$).

Electron density (contoured at 0.8σ) from $2F_o$-$F_c$ maps calculated with model phases (labeled as $2F_o$) or composite annealed omit maps calculated with phases in which the model was omitted to reduce model bias (Adams, P. D. *et al.* Acta Crystallogr D Biol Crystallogr 66, 213-221, 2010) (labeled as Omit) shown for PNGSs in the 3.9Å and the 3.5Å IOMA–10-1074–BG505 structures (Table 1). Glycan residues built into the electron density are shown as colored sticks (fucose, red; GlcNAc, blue; mannose, green; galactose, yellow; sialic acid, purple). We identified complex-type *N*-glycans primarily through the presence of electron density for a core fucose residue. Although the structures were extensively refined (see Methods), coordinates for glycans in our structures should be regarded as approximate: the glycan density was sometimes ambiguous, as expected given the large degree of glycan heterogeneity in HIV-1 Env, one of the most heavily glycosylated proteins known (Doores, K. J. FEBS J 282, 4679-4691, 2015). (**b**) Schematic versions of crystallographically-identified BG505 SOSIP.664 glycans (fucose, red triangle; GlcNAc, blue square; mannose, green circle; galactose, yellow circle; sialic acid, purple diamond) shown in panel a (labeled as 3.9Å and 3.5Å) compared with glycans from the 4.2Å EM structure of a natively-glycosylated JR-FL (non-SOSIP) Env (Lee, J. H., Ozorowski, G. & Ward, A. B. Science 351, 1043-1048, 2016), the 3.7Å crystal structure of a high mannose-only fully- but not natively-glycosylated BG505 SOSIP.664 (Stewart-Jones, G. B. E. *et al.* Cell 165, 813-826, 2016), and a mass spectroscopy analysis of natively-glycosylated BG505 SOSIP.664 (Behrens, A. J. *et al.* Cell Reports 14, 2695-2706, 2016). Not all glycan species identified at each PNGS by mass spectroscopy (Behrens, A. J. *et al.* Cell Reports 14, 2695-2706, 2016) are shown; the major species are depicted in this figure except at PNGSs in which it appears that our crystals contained a subset of BG505 SOSIP.664 protein with underrepresented glycan species (see text). Although the BG505 SOSIP.664 construct (Sanders, R. W. *et al.* PLoS Pathog 9, e1003618, 2013) was used both for our structures and the mass spectrometry analysis (Behrens, A. J. *et al.* Cell Reports 14, 2695-2706, 2016), some differences in glycans at individual PNGSs between the mass spectrometry study and our structures might be expected if the crystals preferentially incorporated a subset of the glycosylation states within the BG505 protein.

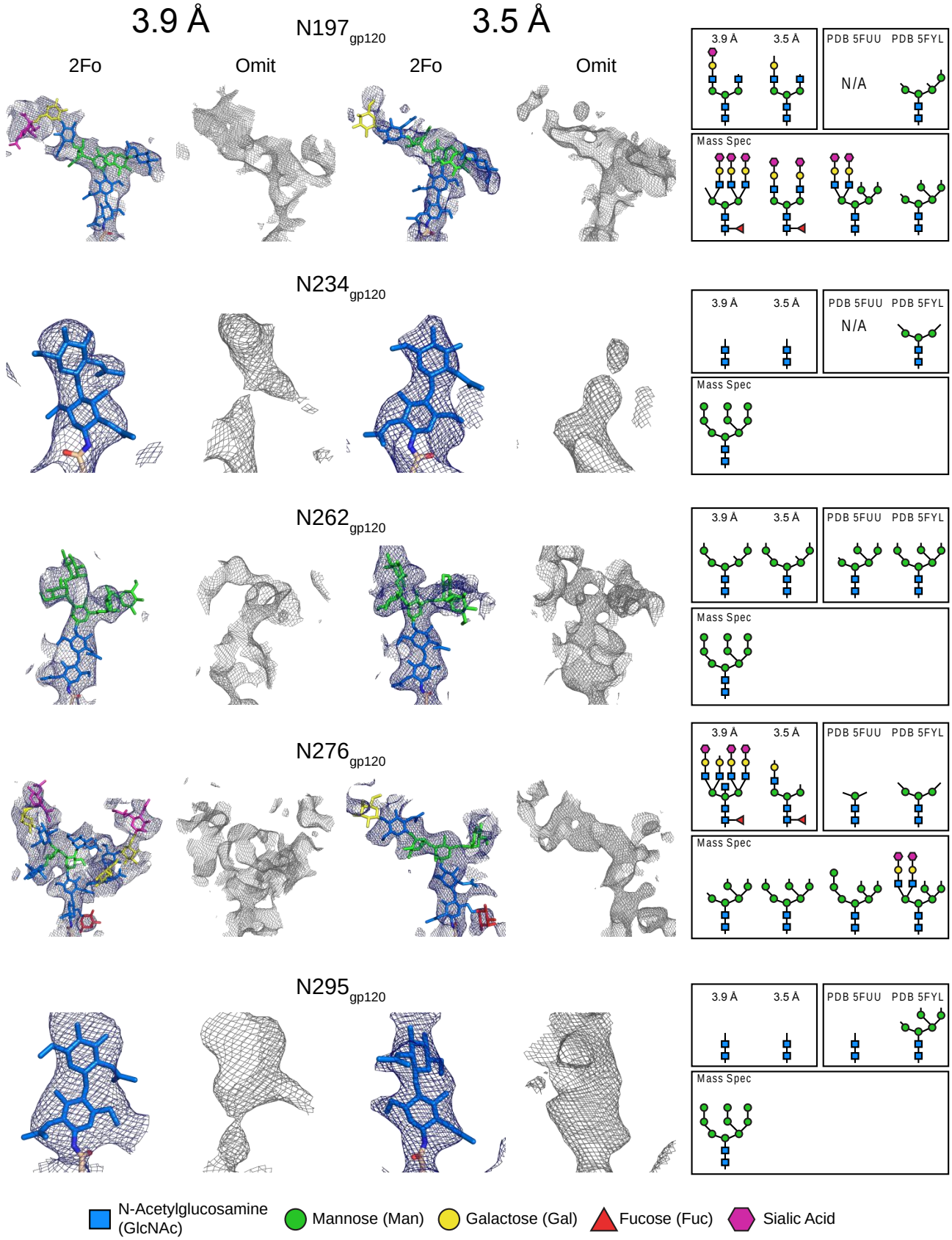


Nature Structural & Molecular Biology: doi:10.1038/nsmb.3291

**Supplementary Figure 6**

Glycans at individual BG505 SOSIP.664 PNGSs ($N197_{gp120}$–$N295_{gp120}$).

Electron density (contoured at 0.8σ) from $2F_o$-$F_c$ maps calculated with model phases (labeled as $2F_o$) or composite annealed omit maps calculated with phases in which the model was omitted to reduce model bias (Adams, P. D. *et al.* Acta Crystallogr D Biol Crystallogr 66, 213-221, 2010) (labeled as Omit) shown for PNGSs in the 3.9Å and the 3.5Å IOMA–10-1074–BG505 structures (Table 1). Glycan residues built into the electron density are shown as colored sticks (fucose, red; GlcNAc, blue; mannose, green; galactose, yellow; sialic acid, purple). We identified complex-type *N*-glycans primarily through the presence of electron density for a core fucose residue. Although the structures were extensively refined (see Methods), coordinates for glycans in our structures should be regarded as approximate: the glycan density was sometimes ambiguous, as expected given the large degree of glycan heterogeneity in HIV-1 Env, one of the most heavily glycosylated proteins known (Doores, K. J. FEBS J 282, 4679-4691, 2015). (**b**) Schematic versions of crystallographically-identified BG505 SOSIP.664 glycans (fucose, red triangle; GlcNAc, blue square; mannose, green circle; galactose, yellow circle; sialic acid, purple diamond) shown in panel a (labeled as 3.9Å and 3.5Å) compared with glycans from the 4.2Å EM structure of a natively-glycosylated JR-FL (non-SOSIP) Env (Lee, J. H., Ozorowski, G. & Ward, A. B. Science 351, 1043-1048, 2016), the 3.7Å crystal structure of a high mannose-only fully- but not natively-glycosylated BG505 SOSIP.664 (Stewart-Jones, G. B. E. *et al.* Cell 165, 813-826, 2016), and a mass spectroscopy analysis of natively-glycosylated BG505 SOSIP.664 (Behrens, A. J. *et al.* Cell Reports 14, 2695-2706, 2016). Not all glycan species identified at each PNGS by mass spectroscopy (Behrens, A. J. *et al.* Cell Reports 14, 2695-2706, 2016) are shown; the major species are depicted in this figure except at PNGSs in which it appears that our crystals contained a subset of BG505 SOSIP.664 protein with underrepresented glycan species (see text). Although the BG505 SOSIP.664 construct (Sanders, R. W. *et al.* PLoS Pathog 9, e1003618, 2013) was used both for our structures and the mass spectrometry analysis (Behrens, A. J. *et al.* Cell Reports 14, 2695-2706, 2016), some differences in glycans at individual PNGSs between the mass spectrometry study and our structures might be expected if the crystals preferentially incorporated a subset of the glycosylation states within the BG505 protein.

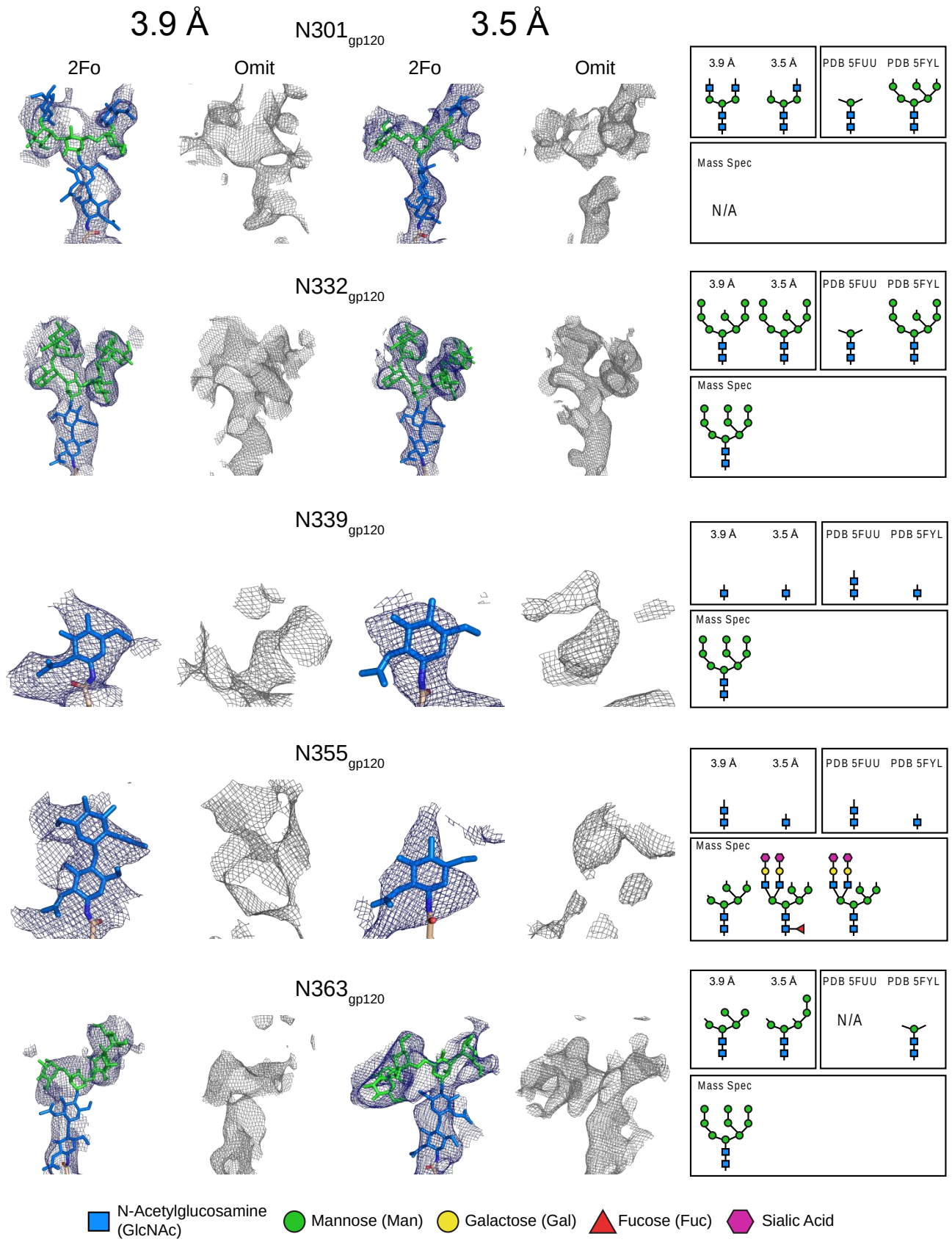


Nature Structural & Molecular Biology: doi:10.1038/nsmb.3291

**Supplementary Figure 7**

Glycans at individual BG505 SOSIP.664 PNGSs ($N301_{gp120}$–$N363_{gp120}$).

Electron density (contoured at 0.8σ) from $2F_o$-$F_c$ maps calculated with model phases (labeled as $2F_o$) or composite annealed omit maps calculated with phases in which the model was omitted to reduce model bias (Adams, P. D. *et al.* Acta Crystallogr D Biol Crystallogr 66, 213-221, 2010) (labeled as Omit) shown for PNGSs in the 3.9Å and the 3.5Å IOMA–10-1074–BG505 structures (Table 1). Glycan residues built into the electron density are shown as colored sticks (fucose, red; GlcNAc, blue; mannose, green; galactose, yellow; sialic acid, purple). We identified complex-type *N*-glycans primarily through the presence of electron density for a core fucose residue. Although the structures were extensively refined (see Methods), coordinates for glycans in our structures should be regarded as approximate: the glycan density was sometimes ambiguous, as expected given the large degree of glycan heterogeneity in HIV-1 Env, one of the most heavily glycosylated proteins known (Doores, K. J. FEBS J 282, 4679-4691, 2015). (**b**) Schematic versions of crystallographically-identified BG505 SOSIP.664 glycans (fucose, red triangle; GlcNAc, blue square; mannose, green circle; galactose, yellow circle; sialic acid, purple diamond) shown in panel a (labeled as 3.9Å and 3.5Å) compared with glycans from the 4.2Å EM structure of a natively-glycosylated JR-FL (non-SOSIP) Env (Lee, J. H., Ozorowski, G. & Ward, A. B. Science 351, 1043-1048, 2016), the 3.7Å crystal structure of a high mannose-only fully- but not natively-glycosylated BG505 SOSIP.664 (Stewart-Jones, G. B. E. *et al.* Cell 165, 813-826, 2016), and a mass spectroscopy analysis of natively-glycosylated BG505 SOSIP.664 (Behrens, A. J. *et al.* Cell Reports 14, 2695-2706, 2016). Not all glycan species identified at each PNGS by mass spectroscopy (Behrens, A. J. *et al.* Cell Reports 14, 2695-2706, 2016) are shown; the major species are depicted in this figure except at PNGSs in which it appears that our crystals contained a subset of BG505 SOSIP.664 protein with underrepresented glycan species (see text). Although the BG505 SOSIP.664 construct (Sanders, R. W. *et al.* PLoS Pathog 9, e1003618, 2013) was used both for our structures and the mass spectrometry analysis (Behrens, A. J. *et al.* Cell Reports 14, 2695-2706, 2016), some differences in glycans at individual PNGSs between the mass spectrometry study and our structures might be expected if the crystals preferentially incorporated a subset of the glycosylation states within the BG505 protein.

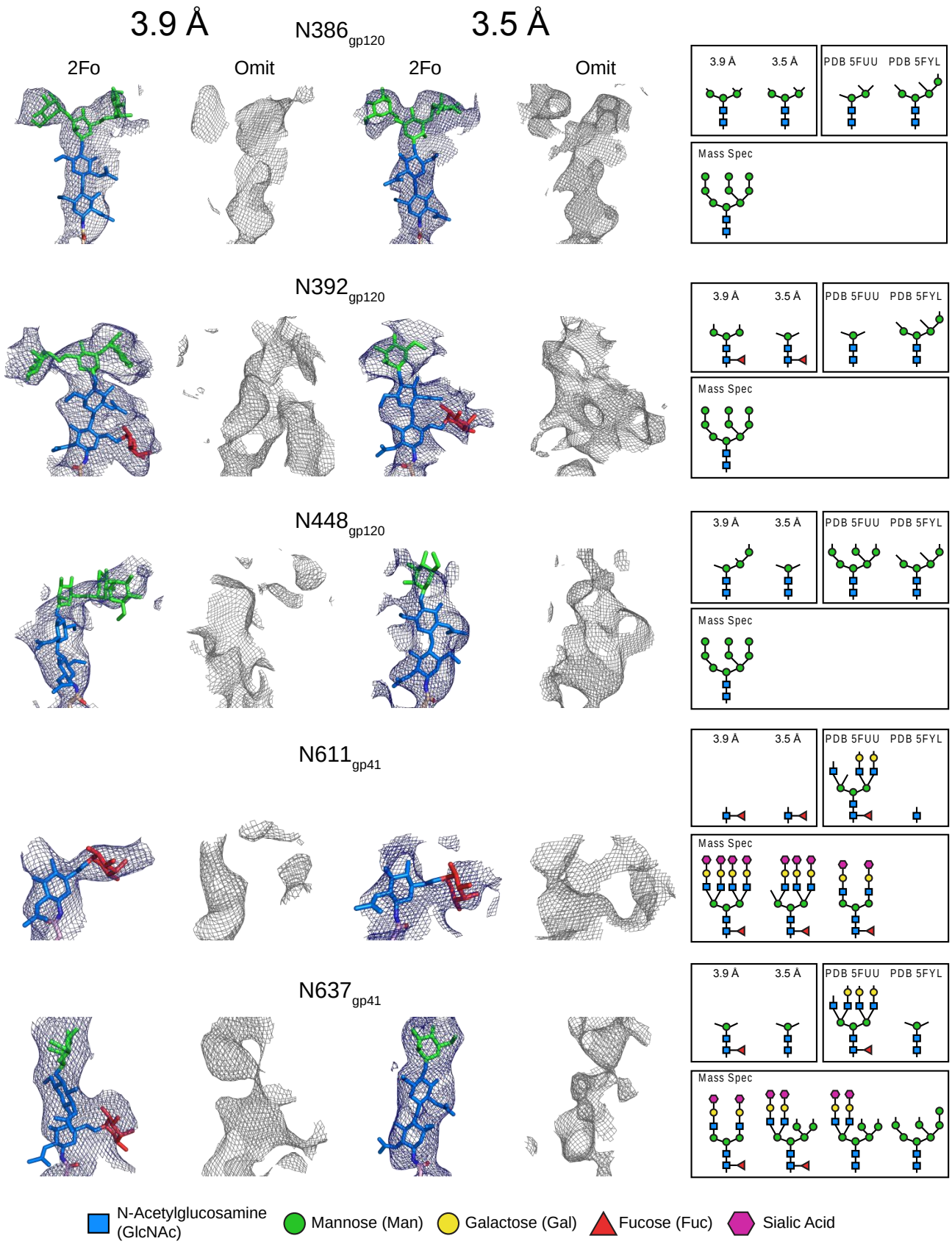
3.9 Å
N386gp120
3.5 Å
2Fo
Omit
2Fo
Omit
3.9 Å
3.5 Å
PDB 5FUU
PDB 5FYL
Mass Spec
N392gp120
N448gp120
N611gp41
N637gp41
N-Acetylglucosamine (GlcNAc)
Mannose (Man)
Galactose (Gal)
Fucose (Fuc)
Sialic Acid

**Supplementary Figure 8**

Glycans at individual BG505 SOSIP.664 PNGSs ($N386_{gp120}$–$N637_{gp41}$).

Electron density (contoured at 0.8σ) from $2F_o$-$F_c$ maps calculated with model phases (labeled as $2F_o$) or composite annealed omit maps calculated with phases in which the model was omitted to reduce model bias (Adams, P. D. *et al.* Acta Crystallogr D Biol Crystallogr 66, 213-221, 2010) (labeled as Omit) shown for PNGSs in the 3.9Å and the 3.5Å IOMA–10-1074–BG505 structures (Table 1). Glycan residues built into the electron density are shown as colored sticks (fucose, red; GlcNAc, blue; mannose, green; galactose, yellow; sialic acid, purple). We identified complex-type *N*-glycans primarily through the presence of electron density for a core fucose residue. Although the structures were extensively refined (see Methods), coordinates for glycans in our structures should be regarded as approximate: the glycan density was sometimes ambiguous, as expected given the large degree of glycan heterogeneity in HIV-1 Env, one of the most heavily glycosylated proteins known (Doores, K. J. FEBS J 282, 4679-4691, 2015). (**b**) Schematic versions of crystallographically-identified BG505 SOSIP.664 glycans (fucose, red triangle; GlcNAc, blue square; mannose, green circle; galactose, yellow circle; sialic acid, purple diamond) shown in panel a (labeled as 3.9Å and 3.5Å) compared with glycans from the 4.2Å EM structure of a natively-glycosylated JR-FL (non-SOSIP) Env (Lee, J. H., Ozorowski, G. & Ward, A. B. Science 351, 1043-1048, 2016), the 3.7Å crystal structure of a high mannose-only fully- but not natively-glycosylated BG505 SOSIP.664 (Stewart-Jones, G. B. E. *et al.* Cell 165, 813-826, 2016), and a mass spectroscopy analysis of natively-glycosylated BG505 SOSIP.664 (Behrens, A. J. *et al.* Cell Reports 14, 2695-2706, 2016). Not all glycan species identified at each PNGS by mass spectroscopy (Behrens, A. J. *et al.* Cell Reports 14, 2695-2706, 2016) are shown; the major species are depicted in this figure except at PNGSs in which it appears that our crystals contained a subset of BG505 SOSIP.664 protein with underrepresented glycan species (see text). Although the BG505 SOSIP.664 construct (Sanders, R. W. *et al.* PLoS Pathog 9, e1003618, 2013) was used both for our structures and the mass spectrometry analysis (Behrens, A. J. *et al.* Cell Reports 14, 2695-2706, 2016), some differences in glycans at individual PNGSs between the mass spectrometry study and our structures might be expected if the crystals preferentially incorporated a subset of the glycosylation states within the BG505 protein.

**a**

| $IC_{50}$ values (μg/mL) | 10-1074 | PGT122 | PGT121 |
|---|---|---|---|
| Mean $IC_{50}$ of strains w/ PNGS 156 | 0.20 (n=75) | 0.19 (n=97) | 0.14 (n=170) |
| Mean $IC_{50}$ of strains w/o PNGS 156 | 0.05 (n=8) | 0.46 (n=7) | 0.03 (n=9) |

**b**

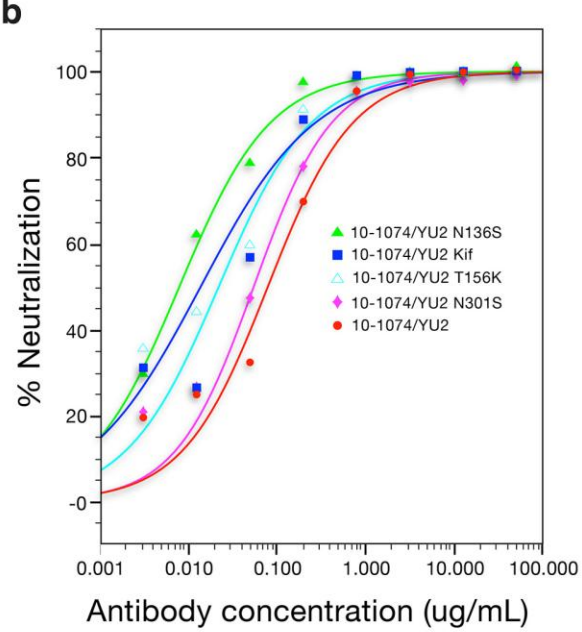


$IC_{50}$ values (mg/mL)

| Strain | 10-1074 |
|---|---|
| YU2 | 0.078 |
| YU2 KIF | 0.014 |
| YU2 N136S | 0.008 |
| YU2 T156K | 0.022 |
| YU2 N197K | 0.043 |
| YU2 N276K | 0.081 |
| YU2 N301S | 0.054 |

**c**

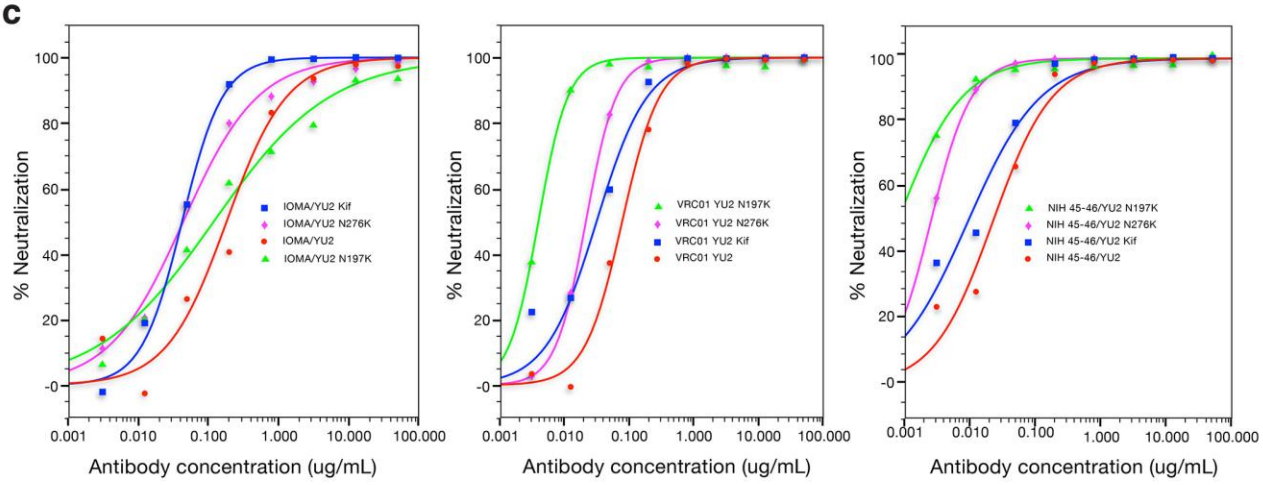


**d**

$IC_{50}$ values (μg/mL)

| Strain | IOMA | VRC01 | NIH45-46 |
|---|---|---|---|
| YU2 | 0.180 | 0.076 | 0.022 |
| YU2 T156K | 0.394 | 0.053 | 0.011 |
| YU2 N136S | 0.120 | 0.039 | 0.012 |
| YU2 N301S | 0.314 | 0.023 | 0.006 |
| YU2 N276K | 0.044 | 0.021 | 0.002 |
| YU2 N197K | 0.119 | 0.004 | 0.001 |
| YU2 KIF | 0.042 | 0.031 | 0.009 |

**Supplementary Figure 9**

Effects of glycans on neutralization potencies of 10-1074 and IOMA.

(**a**) Effects of an intact PNGS at $N156_{gp120}$ on PGT121-family bNAbs. Geometric mean $IC_{50}$s (μg/mL) of 10-1074, PGT122, and PGT121 were calculated for HIV-1 strains with or without a PNGS at $N156_{gp120}$. Only strains containing a PNGS at $N332_{gp120}$ were included in this analysis. Mean $IC_{50}$s are calculated treating >50 μg/mL values as 50 μg/mL. PGT122 was ~2-fold more potent against strains including the $N156_{gp120}$ PNGS, whereas 10-1074 showed ~4-fold greater potency against viral strains lacking the $N156_{gp120}$ PNGS. PGT121 also was more potent against strains lacking PNGS $N156_{gp120}$. PGT122 has CDRL3 residue $95R_{LC}$, while 10-1074 and PGT121 have Ser and Val at position $95_{LC}$, respectively. $IC_{50}$ values are those reported in the following references: Mouquet, H. *et al.* Proc Natl Acad Sci USA 109, E3268-3277, 2012; Sok, D. *et al.* Science Translational Medicine 6, 236ra263, 2014; Walker, L. M. *et al.* Nature 477, 466–470, 2011; Ferguson, A. L. *et al.* PLoS One 8, e80562, 2013; Huang, J. *et al.* Nature 515, 138-142, 2014. (**b**) Effects of glycan deletions at $N137_{gp120}$, $N156_{gp120}$, and $N301_{gp120}$ on 10-1074 neutralization. In vitro neutralization assays were conducted with HIV-$1^{YU2}$ pseudoviruses that included all glycans (listed as YU2), had introduced mutations to remove the $N137_{gp120}$ glycan (YU2 N137S), the $N156_{gp120}$ glycan (YU2 N156K), the $N301_{gp120}$ glycan (YU2 N301S), or included all glycans in a high mannose form (YU2 Kif). (**c,d**) Comparison of glycosylation deletions on neutralization by IOMA and VRC01-class bNAbs (VRC01 and NIH45-46). In vitro neutralization assays were conducted with HIV-$1^{YU2}$ pseudoviruses that included all glycans (listed as YU2), had introduced mutations to remove the $N276_{gp120}$ glycan (YU2 N276K), the $N197_{gp120}$ glycan (YU2 N197K), or included all glycans in a high mannose form (YU2 Kif). Removal of glycans or conversion to high-mannose-only glycans had no effect (PNGS $N197_{gp120}$) or increased IOMA's neutralization potency by ~4-fold (PNGS $N276_{gp120}$ and high-mannose-only glycans). For VRC01-class bNAbs, the same changes produced ~20-fold increased potency (PNGS $N197_{gp120}$), ~4-11–fold increased potency (PNGS $N276_{gp120}$), or ~2-fold increased potency (high-mannose-only glycans).

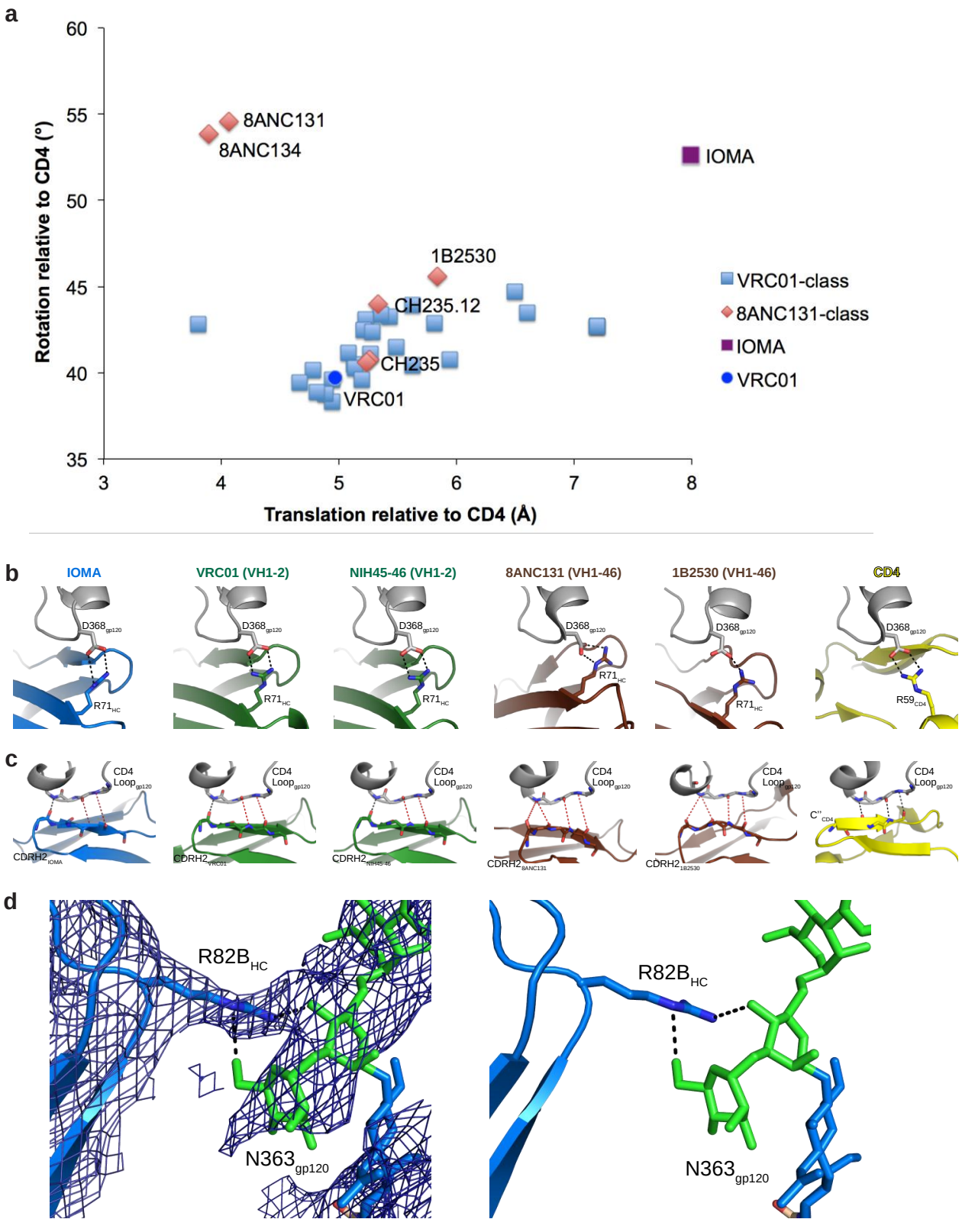
a
Rotation relative to CD4 (°)
Translation relative to CD4 (Å)
8ANC131
8ANC134
1B2530
CH235.12
CH235
VRC01
IOMA
VRC01-class
8ANC131-class
IOMA
VRC01
b
IOMA
VRC01 (VH1-2)
NIH45-46 (VH1-2)
8ANC131 (VH1-46)
1B2530 (VH1-46)
CD4
c
d
R82B$_{HC}$
N363$_{gp120}$

**Supplementary Figure 10**

Comparisons of IOMA, VH1-2/VRC01-class, and VH1-46-class bNAbs.

(**a**) Rotation angle and translation distance of $V_H$ domains of VH1-2 and VH1-46 CD4bs bNAbs in complex with Env (gp120 or trimer) relative to CD4 in complex with HxBc2 gp120 (PDB code 1GC1). Data points for complexes of VRC01-like bNAbs are shown as blue squares; complexes of 8ANC131-like bNAbs are shown as red diamonds; IOMA is shown as a purple square; VRC01 is shown as a blue circle. (**b**) Interactions of Env residue $D368_{gp120}$ with IOMA residue $R71_{HC}$ and indicated bNAbs and with CD4 residue $R59_{CD4}$. Black dashed lines indicate potential hydrogen bonds; red dashed lines indicate potential hydrogen bonds with non-ideal geometry. (**c**) Interactions of the CD4-binding loop in gp120 with CDRH2 of IOMA and indicated bNAbs and with the C" strand of CD4. Black dashed lines indicate potential hydrogen bonds; gray dashed lines indicate potential hydrogen bonds with non-ideal geometry. (**d**) IOMA's interaction with *N*-glycan attached to $N363_{gp120}$. $R82B_{HC}$ interacts with the core pentasaccharide of the $N363_{gp120}$ glycan. Top: $2F_o$-$F_c$ electron density map (contoured at $0.8\sigma$) superimposed over coordinates (glycans colored as in Supplementary Figs. 5–8). Bottom: coordinates alone.

## Supplementary Note

Sequence alignment of IOMA, VRC01, and 8ANC131 HCs and LCs with their respective germline V gene segment sequences.